Dalton Transactions

ROYAL SOCIETY OF CHEMISTRY

PAPER

View Article Online
View Journal | View Issue

Cite this: *Dalton Trans.*, 2025, **54**, 16836

Synthesis and cytotoxic activity of morpholino-*s*-triazine derivatives of POCOP-Ni(II) pincers

Juan S. Serrano-García, [a] Andrés Amaya-Flórez, [a] Antonino Arenaza-Corona, [a] María Teresa Ramírez-Apan, [a] Adrián L. Orjuela, †[b] Jorge Alí-Torres, [b] Marcos Flores-Alamo, [c] Simón Hernandez-Ortega, [a] Patricia Cano-Sanchez [a] and David Morales-Morales *[a]

Received 5th June 2025,
Accepted 14th October 2025

DOI: 10.1039/d5dt01322d

rsc.li/dalton

Six POCOP-Ni(II) complexes (**2**, **3a**, **3b**, **4**, **5**, and **6**) bearing a morpholino-*s*-triazine moiety were synthesized and fully characterized. The structures of complexes **2** and **3a** were determined by single-crystal X-ray diffraction, revealing a distorted square-planar geometry around the metal center. Based on these structures, a supramolecular analysis using Hirshfeld surfaces was also carried out, identifying intermolecular hydrogen bonding and π···π stacking interactions. The antiproliferative activity of all complexes was evaluated against six cancer cell lines and a non-cancerous cell line (COS7). Complexes **3a** and **3b** exhibited the highest antiproliferative activity mainly against leukemia (K562), with IC_{50} values of 0.55 ± 0.04 μM and 0.59 ± 0.04 μM, respectively. A study of the mechanism of action includes competitive displacement of ethidium bromide (EB) fluorescence within DNA, and molecular docking with DNA and PI3K.

1. Introduction

Cancer refers to a broad group of diseases characterized by the abnormal growth of cells.[1] In 2022, the WHO reported 20 million new cases and nearly 10 million deaths from this disease worldwide, making it a major public health problem in the 21[st] century,[2] and thus, the development of new therapeutic strategies is imperative based on these alarming statistics. Chemotherapy is currently one of the most widely used treatments against cancer.[3] However, commercial drugs such as cisplatin present adverse effects, often due to a lack of selectivity.[4,5] This underscores the importance of ongoing research into new anticancer drugs.

Pincer-type compounds are known for their high thermal and chemical stability, leading to their extensive use in fields such as catalysis.[6–9] However, since the discovery of an SCN-Ni(II) pincer in the active site of the enzyme lactate racemase, the application of these compounds as agents with biological activity has gained importance.[10,11] Recently, our research group has reported a series of POCOP-Ni(II) pincer compounds derived from fluoroglucinol and their *para*-acetylated derivatives, exhibiting IC_{50} values ranging from 2.43 to 14.36 μM against the U251, K562, HCT-15, SKLU-1, and MCF-7 cell lines.[12,13] Among them, complexes bearing the isopropyl group like **1** exhibit higher levels of cytotoxicity (Fig. 1).

The cytotoxic activity or selectivity of metal complexes could be increased by incorporating fragments with biological activity, such as triazines.[14,15] 1,3,5-Triazine, also known as *s*-triazine, is the symmetric isomer of a six-membered aromatic

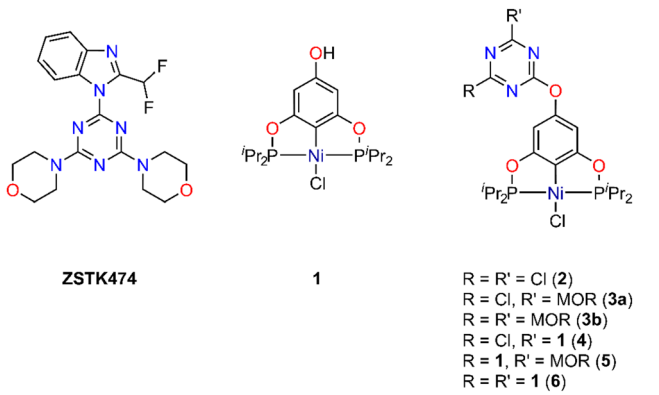

Fig. 1 The PI3K inhibitor ZSTK474, a POCOP-Ni(II) pincer complex (**1**) previously reported,[13,31] and POCOP-Ni(II) pincer complexes evaluated in this work as antitumoral agents (**2**–**6**).

[a]*Instituto de Química, Universidad Nacional Autónoma de México, Circuito Exterior, Ciudad de México, CP 04510, Mexico. E-mail: damor@unam.mx; Fax: +52-55-56162217; Tel: +52-55-56224514*
[b]*Departamento de Química, Universidad Nacional de Colombia-Sede Bogotá, 111321, Colombia*
[c]*Facultad de Química, División de Estudios de Posgrados, Universidad Nacional Autónoma de México, Circuito Exterior, CU, 04510, Mexico*
†Current address: Instituto de Investigaciones Científicas y Servicios de Alta Tecnología (INDICASAT AIP), Panama City, Panama.

ring containing three nitrogen atoms alternating with three carbon atoms. Due to its versatility, this compound has been widely used in the synthesis of new compounds with potential anticancer activity. Usually, 2,4,6-trichloro-*s*-triazine (TCT) or cyanuric chloride is preferred as a starting material due to its temperature-dependent reactivity, allowing control over the number of substitutions.[3,16–22]

The compound ZSTK474, a *s*-triazine derivative, has been highlighted since it is an inhibitor of phosphoinositide 3-kinases (PI3Ks), lipid enzymes that play a significant role in regulating the growth, proliferation, and metastasis of cancer cells. ZSTK474 is currently in Phase I/II clinical trials for the treatment of solid tumors.[23–27] This compound contains two morpholine (MOR) subunits, a six-membered heterocycle with ether and amino functional groups. The presence of the nitrogen atom enables donor–acceptor interactions, creating strong substrate–receptor bonds, and this is the reason why this fragment has been widely used in compounds with biological activity.[28–30]

Based on the above, we report herein a series of six new compounds using the *s*-triazine scaffold, evaluating the relationship between cytotoxic activity and the number of POCOP-Ni(II) pincer and morpholine subunits.

2. Results and discussion

Pincer **1** was synthesized following the methodology previously reported by our research group.[31] The morpholino-*s*-triazine derivatives were obtained from the reaction of **1**, morpholine (MOR), and 2,4,6-trichloro-*s*-triazine (TCT); derivatives without morpholine were also prepared for comparison purposes (see Scheme 1 and the Experimental section). Although similar compounds have been reported by our investigation group, the methodology was improved by eliminating the N_2 atmosphere requirement and employing lower temperatures for mono- and disubstituted derivatives.[32]

All compounds were characterized by ^{1}H, $^{13}C\{^{1}H\}$, and $^{31}P\{^{1}H\}$ NMR spectroscopy, MS (DART^{+}, MALDI), ATR-FTIR, and elemental analysis, yielding the expected signals. Given the structural similarity of **2**, **4**, and **6** complexes, their ^{1}H NMR signals were similar as well, showing a small displacement to higher ppm for the aromatic signal (δ 6.26–6.31) as the substitution degree on the triazine increased. ^{1}H NMR signals corresponding to the morpholine fragment were observed from 3.60 ppm to 3.85 ppm for **3a**, **3b** and **5** complexes. For complex **3a**, the ^{1}H and ^{13}C NMR spectra showed non-equivalent protons and carbons of the morpholine fragment. This resolution phenomenon could be associated with a combination of rigidity *via* π-delocalization of the N atom and the non-symmetry of the triazine ring with its different substituents.

The molecular structures of complexes **2** and **3a** were unequivocally elucidated through single crystal X-ray diffraction analysis. Suitable crystals were obtained for compound **2** from a 1 : 1 CH_2Cl_2/hexane solution and for compound **3a** from a 2 : 1 hexane/acetyl acetate solution. The results show that compound **2** crystallises in a *monoclinic* system with the *Cc* space group, while compound **3a** adopts a *triclinic* system

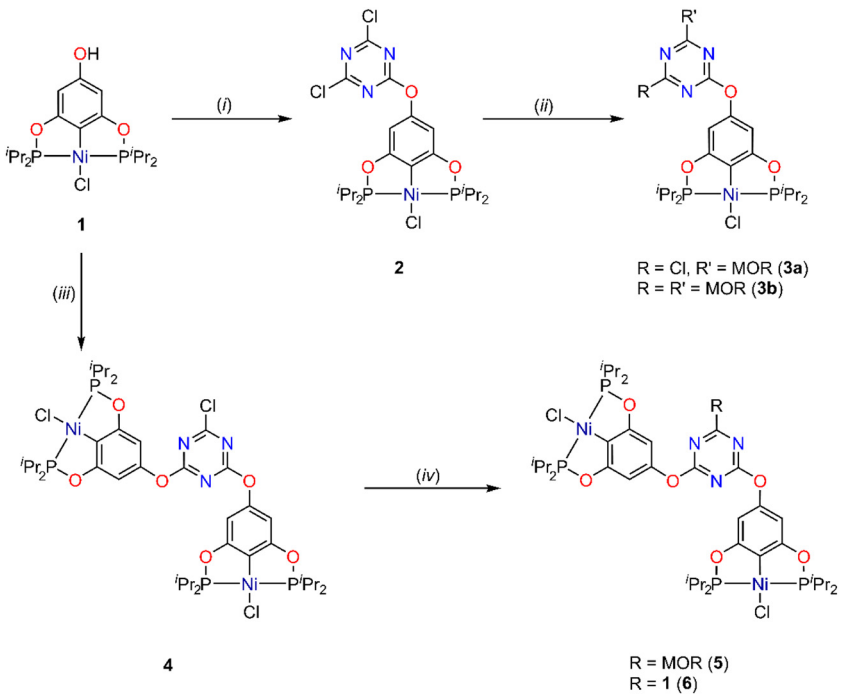

Scheme 1 Synthesis of morpholino-*s*-triazine derivatives of POCOP-Ni(II) pincers. (i) TCT, DIPEA, THF, 0 °C. (ii) MOR (1 or 2 equiv.), DIPEA, acetone, T = −5 °C (**3a**) or 55 °C (**3b**), 1 d. (iii) TCT, DIPEA, CH_2Cl_2, 25 °C, 1 d. (iv) MOR and DIPEA (**5**) or 1 and Na_2CO_3 (**6**), acetone, 56 °C, 1 d. MOR = morpholine, TCT = 2,4,6-trichloro-*s*-triazine, DIPEA = diisopropylethylamine.

with the $P\bar{1}$ space group. The two compounds contain a single molecule on their corresponding asymmetric units, as shown in Fig. 2. Molecular structures were visualised and drawn using OLEX2 v1.5.[33] The crystallographic data of the structures are summarised in Table S1. In both compounds, the metal atoms are four-coordinated by two phosphorous, carbon, and chlorine atoms. The resulting geometry around the metal is a distorted square planar. In complex **3a**, the morpholine substituent on the triazine ring adopts the most stable configuration for a saturated six-membered cycle. The selected distances and angles are summarised in Table 1.

Both compounds exhibit non-covalent interactions supported by CH···Cl, CH···N CH···O, and CH···π. The relevant interaction parameters are listed in Table S2. In the crystal structure of **2**, the molecules are settled in chains running along the *b*-axis, which are connected *via* a chlorine atom ($C_{10}H_{10}\cdots Cl_2$) (Fig. 3). Hydrogen atoms not involved in intermolecular interactions are excluded for clarity. The molecular packing of **3a** is stabilised by a tetramer supported by two CH···O and two CH···N interactions. Additionally, π···π stacking is observed between two triazine rings, which is further confirmed by Hirshfeld surface analysis (*vide infra*). The descriptors (hydrogen bonding patterns) were determined using the Mercury program[34] *via* the set graph analysis in each structure.[35] These two interactions were well defined by the two graphic descriptors found [C(12) and $R_4^4(22)$].

To further analyse the intermolecular interactions within the crystalline packaging, Hirshfeld surfaces[36] were calculated using the computer software CrystalExplorer[37] based on the CIF data of the structures. The surfaces were computed using the d_{norm} function and shape index (refer to Fig. 4a–d); in the first case, the red area (indicating close contacts less than the sum of van der Waals radii) of the surface is consistent with the hydrogen bonding characteristics observed near the aromatic ring and propyl group, indicating a CH···π interaction. The shape index function for compound **2** revealed halogen···π interactions (yellow circle); in addition, for **3a** π···π stacking (yellow dotted circle) was found. In addition, the 2D fingerprint[38] plots from the Hirshfeld surfaces were calculated as another tool to evaluate the individual contribution of each type of contact.[39] The most significant contributions were C···H/H···C and Cl···H/H···Cl, which were like two symmetric wings and spikes, respectively, in contrast, H···H contacts contributed the highest percentage to the interactions, followed by N···H/H···N and O···H/H···O (see Table S3 and Chart S1, which summarise the percentages of individual contributions for each contact).

Table 1 Selected bond and angles of the compounds **2** and **3a**

Bond (Å)	**2**	**3b**
Ni–P(1)	2.1532(16)	2.1516(9)
Ni–P(2)	2.1480(15)	2.1501(9)
Ni-Cl(1)	2.1834(15)	2.1925(8)
Ni–C(1)	1.877(5)	1.880(3)
Angle (°)		
P(1)–Ni–P(2)	164.74(6)	164.33(3)
C(1)–Ni–Cl(1)	177.55(19)	176.28(8)
P(1)–Ni–Cl(1)	99.23(6)	97.62(3)
P(2)–Ni–Cl(1)	95.78(6)	97.99(3)
C(1)–Ni–P(1)	82.04(18)	82.04(8)
C(1)–Ni–P(2)	82.86(18)	82.29(8)

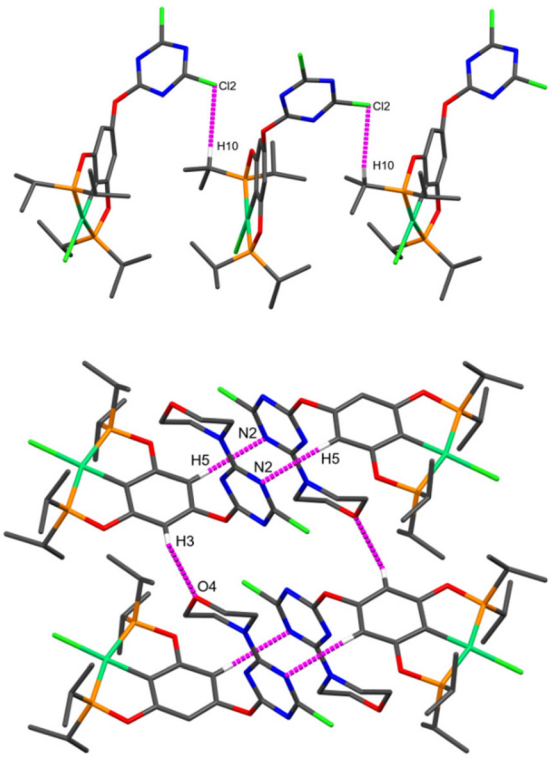

Fig. 3 Polymeric and tetrameric networks supported by non-covalent interactions (purple dashed lines) in compounds **2** (top panel) and **3a** (bottom panel) [set graph descriptor: C(12) and $R_4^4(22)$]. Hydrogen atoms not involved in the interaction were omitted.

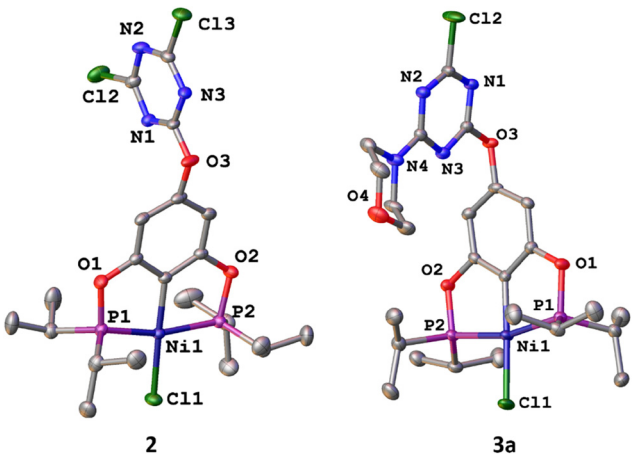

Fig. 2 Molecular structures of **2** (left panel) and **3a** (right panel). The ellipsoids are shown at a 50% probability level and hydrogen atoms have been omitted for clarity.

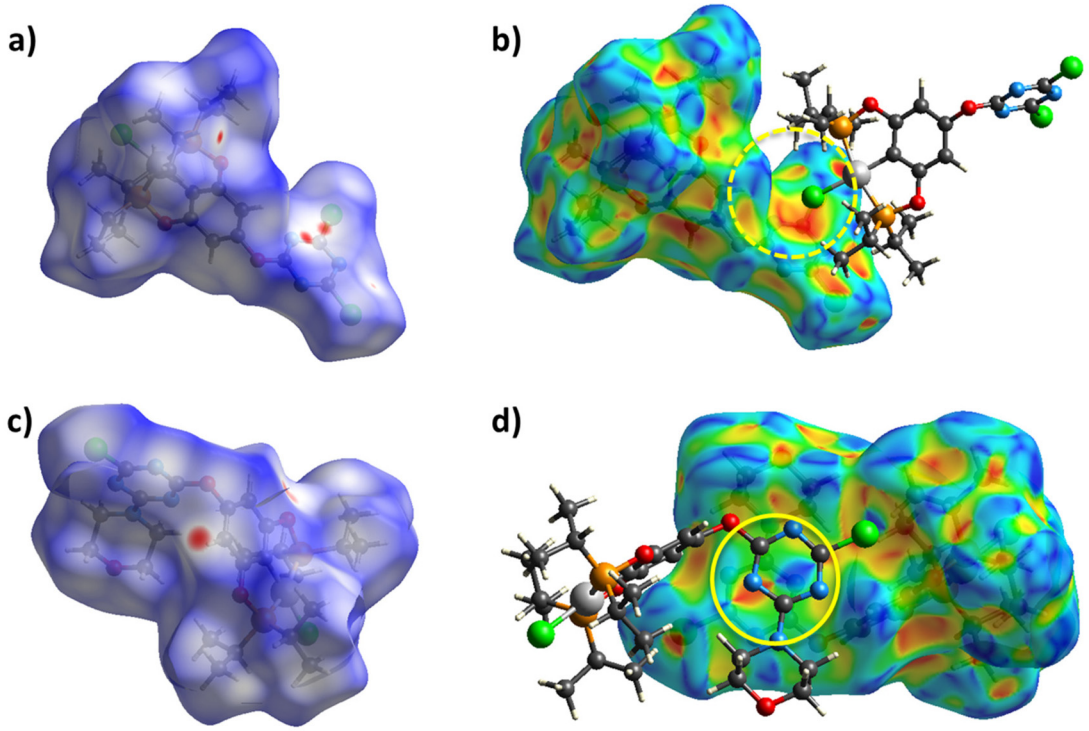

Fig. 4 Hirshfeld surface over the d_{norm} function of compounds **2** (a) and **3a** (c), and over the shape index (b and d) of the complexes respectively.

The information obtained from this supramolecular analysis could be further employed to trace the quantitative and qualitative structure–activity relationships of the biological activity of these compounds.[40–42] In our study, the presence of the morpholine moiety did not increase the percentage of X···H/H···X (X = C, N, and Cl) interactions, except for a slight increase in the O···H/H···O. However, there was a significant increase in the number of H···H/H···H interactions, which coincided with a higher antiproliferative activity (*vide infra*).

3. Cytotoxic activity

The cytotoxic activity of all complexes was preliminarily evaluated *in vitro* against several cancer cell lines and a healthy cell line (the COS7 cell line from African green monkey kidney cells). The assay was performed employing the sulforhodamine B protocol with 10 μM of the corresponding complex for 48 h and six cancer cell lines: HCT-15 (human colorectal adenocarcinoma), MCF-7 (human mammary adenocarcinoma), K562 (human chronic myelogenous leukaemia), U251 (human glioblastoma), PC-3 (human prostatic adenocarcinoma), and SKLU-1 (human lung adenocarcinoma). The results are shown in Table 2. Growth inhibition percentages at the same metal concentration (10 μN) for complexes **4**, **5**, and **6** are presented in Table S4. The decrease in the cytotoxic activity correlated with the reduction of the molar concentration, suggesting that complexes did not rupture into cytotoxic fragments unlike complex **1**.

The cytotoxicity of complexes **2**, **4**, and **6** decreased in proportion to the number of chlorine atoms substituted on the triazine ring. This trend was also observed between the bimetallic complexes **4** and **5**, where the substitution of a chlorine atom by a morpholine fragment on the triazine ring reduced the cytotoxicity, mainly against K562, MCF-7, and COS7. In contrast, the antiproliferative activity of monometallic complexes increased with the amount of morpholine fragments, with the cytotoxicity order being **3b** > **3a** > **2**. The most cytotoxic complexes were **3a** and **3b**, which showed growth inhibition percentages of up to 100% at 10 μM for all cancer cell lines, excluding U251. Selectivity towards the K562 cell line was observed at 1 μM for both **3a** and **3b**. The stability of **2**, **3a**, and **3b** was monitored by UV/vis spectroscopy for 24 h at 10 μM in a PBS solution, containing 0.1% DMSO (Fig. S25–S27). No significant shifts or the appearance of new bands were observed over time, suggesting that the structures of the complexes remain intact under the assay conditions.

IC_{50} values were determined against K562 for complexes **3a** and **3b** owing to their high cytotoxicity and also for complex **2** for comparison purposes (Table S5). As expected, complex **2** presented the highest IC_{50} value (4.96 ± 0.03 μM); however it is lower than that previously reported for complex **1** (5.81 ± 0.2 μM), indicating that the triazine moiety increases the cytotoxicity of the Ni(II) pincer complex.[13] Subsequently, complexes **3a** and **3b** showed similar IC_{50} values (0.55 ± 0.04 and 0.59 ± 0.04 μM, respectively), which are lower than that of cisplatin (1.2 ± 0.08 μM). This high toxicity could be related to a synergistic effect of POCOP-Ni(II) and the morpholino-*s*-triazine

Table 2 Growth inhibition percentage of cancer cell lines by pincer complexes (10 μM). COS7 is a healthy cell line

Compound	U251	PC-3	K562	HCT-15	MCF-7	SKLU-1	COS7
2	23.9	0	69.8	45.2	45.6	14.9	25.9
3a	77.5	100	99.2	100	100	100	100
3a[a]	13.8	20.1	26.6	22.1	12.8	13.4	15.3
3b	75.3	100	97.8	100	92.9	100	100
3b[a]	23.4	38.8	100	20.2	38.3	42.2	39.6
4	3.9	0.9	22.8	1.7	19.6	7.0	17.5
5	5.2	8.5	6.2	0	6.0	0	6.0
6	0	0	0	2.1	4.5	0	0
Cisplatin	92.3	42.9	66.4	38.3	56.2	85.1	66.5

[a] 1 μM.

fragment, which is also exhibited in ZSTK474. Additionally, IC_{50} values were determined against the healthy cell line (COS7). These values ranged from 1.81 to 9.39 μM and were higher than their corresponding values against K562, showing a lower cytotoxicity against the healthy cell line.

4. Ethidium bromide displacement assay

The ethidium bromide (EB) displacement assay was performed through a competitive EB fluorescence titration to evaluate possible intercalations of complexes within DNA. As shown in Fig. S28, the fluorescence intensity of the EB–DNA adduct progressively decreased as the concentration of **2**, **3a**, and **3b** increased from 0 to 0.33 μM, from 0 to 3.3 μM, and from 0 to 0.1 μM, respectively. Higher concentrations could not be explored further due to precipitation. The fluorescence intensity decrease indicates that complexes **2**, **3a**, and **3b** were able to intercalate within the DNA double helix, releasing EB. Spectroscopic measurements showed good linearity in all cases and K_{SV} values for the quenching of fluorescence were calculated from the corresponding Stern–Volmer plot. The K_{SV} values ranged from 1.5×10^7 to 3×10^8 M^{-1}, following the order **3a** > **2** > **3b**. Those values are significantly lower than those of the starting pincer **1** (2.8×10^9 M^{-1}), suggesting that *s*-triazine fragment incorporation would lower the intercalation ability of the POCOP-Ni(II) pincer.[13]

5. Computational results

As observed in Fig. 5, there is a slight difference between the crystal structures of the nickel complexes and the DFT-optimized geometries, reflected in an RMSD greater than 1 Å (a side view is shown in Fig. S29). This deviation can be attributed to the absence of crystal packing forces in DFT optimization, allowing the complex to relax to a lower-energy conformation in the gas phase or solvent model. Additionally, the solvent effect included in the optimization process alters the electrostatic environment, further contributing to structural relaxation and subtle changes in bond angles and distances. These differences highlight the influence of crystal lattice constraints and solvation on molecular geometry.

5.1. Molecular docking of PI3K kinase

Phosphoinositide 3-kinases (PI3Ks) are enzymes involved in essential cellular functions such as cell growth and proliferation. Inhibition of PI3Ks (*e.g.* PI3Kγ inhibition) has shown

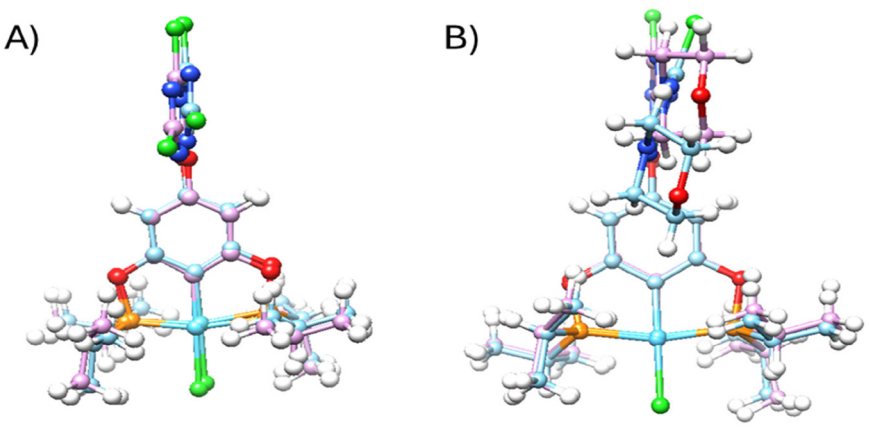

Fig. 5 Superposition of the crystal structure (light blue) and DFT-optimized geometry (purple) for (A) **2** and (B) **3a** complexes. Atom color codes: Cl (green), H (white), O (red), N (cyan), Ni (light blue), and P (orange).

promising anticancer activity.[43,44] For molecular docking, the target was the catalytic subunit (p110γ) of PI3Kγ with inhibitor 6K5 as a reference (PDB code 5JHB).[45,46] As observed in Table 3, the binding affinities of the nickel complexes are higher than that of the reference compound, a potent kinase inhibitor, which suggests that these complexes may exhibit inhibitory activity. This is further supported by experimental data, indicating a correlation between calculated binding energies and observed biological activities.

For complex **2**, two hydrogen bond interactions were identified with ASP264 and ASP836. The binding site for this complex differs from that of the other complexes due to its polar head, which includes chlorinated substituents on the *s*-triazine ring. This distinct orientation enhances specific hydrogen bonding and polar interactions in the active site, contributing to a unique binding profile.

In contrast, the **3a** complex exhibits substantial hydrophobic interactions with the phosphine groups, interacting with residues such as Ala805, Met804, Pro810, and Lys890. Additionally, the *s*-triazine ring facilitates π-alkyl interactions with Ile 831 and Ile879 and a T-shaped interaction with Tyr867. These interactions are predominantly aromatic, distinguishing them from the interactions observed with **2** and indicating a different binding mode, as shown in Fig. 6.

For complex **3b**, the binding site and hydrophobic interactions are like those of **3a**. However, **3b** forms two additional hydrogen bonds with ASN951 and ASP964, which correlates with its higher binding energy, suggesting a stronger interaction with the target.

Table 3 Binding energies of nickel complexes with phosphoinositide 3-kinase PI3Kγ (p110γ subunit) compared to the reference inhibitor (6K5). (PDB code 5JHB)

	Ref.	2	3a	3b
Binding energy (kcal mol^{-1})	−6.54	−7.00	−9.46	−9.64

5.2. Molecular docking of DNA

In addition to their binding affinities with phosphoinositide 3-kinases, the nickel complexes were also evaluated for their interaction with DNA, as shown in Table 4. The calculated binding energies indicate that all nickel complexes exhibit stronger interactions with DNA compared to cisplatin, a well-

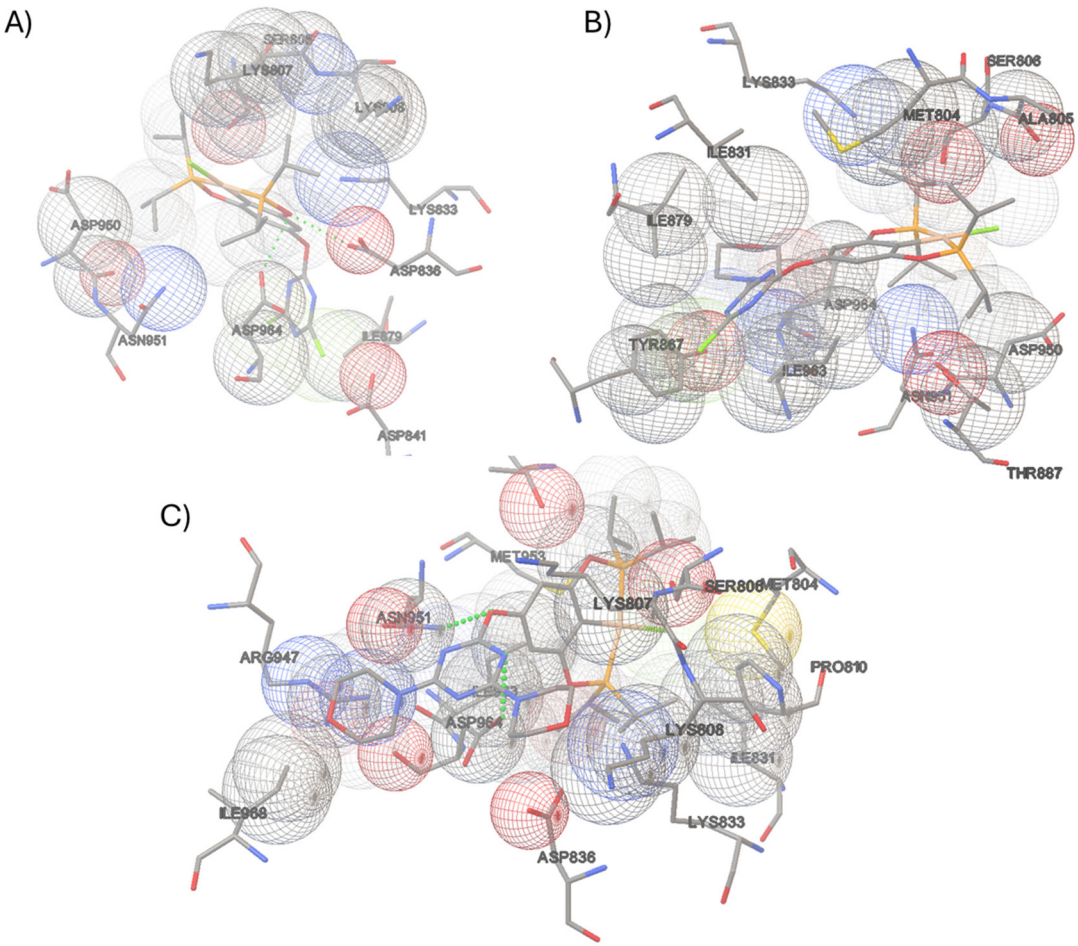

Fig. 6 Molecular interactions between phosphoinositide 3-kinase PI3Kγ (p110γ subunit) and (A) **2**, (B) **3a**, and (C) **3b** complexes. Color code: Ni (cream), N (blue), O (red), C (gray), S (yellow), Cl (green), and P (orange). Green dashed lines represent hydrogen bonds.

Table 4 Binding energies of nickel complexes with DNA (PDB code 1AIO) compared to cisplatin

	Cisplatin	2	3a	3b
Binding energy (kcal mol^{-1})	−5.64	−6.86	−8.87	−9.71

known DNA-targeted anti-cancer agent, with binding energies of −6.86, −8.87, and −9.71 kcal mol^{-1} for **2**, **3a**, and **3b**, respectively, compared to −5.64 kcal mol^{-1} for cisplatin. This trend, consistent with the kinase binding data, suggests that the increased stability and affinity of the nickel complexes for both targets could translate into enhanced biological activity. Complexes **3a** and **3b** show notably high binding energies, reinforcing their potential as dual-target inhibitors with significant anti-cancer activity across both DNA and kinase pathways.

The interaction of the phosphine groups in the nickel complexes is primarily hydrophobic (Fig. 7), consistent with similar behavior noted in their interactions with the 3-kinase receptor. Despite their shared hydrophobic character, all three complexes (**2**, **3a**, and **3b**) exhibit the same coordination mode within the DNA binding site. However, complex **2** shows a unique behavior due to the *s*-triazine ring with chlorine substituents, which generates electrostatic repulsion with the phosphate backbone of the DNA. This repulsive interaction may lead to decreased binding stability and affinity for DNA, potentially impacting the effectiveness of **2** in targeting DNA.

In contrast, complexes **3a** and **3b** demonstrate enhanced binding stability due to favorable electrostatic interactions with the DNA backbone. These interactions contribute to stabilization of a preferred DNA binding conformation, where the electrostatic attraction between the complex and the negatively charged phosphate groups reinforces the overall complex stability. This increased stability in the DNA binding site, particularly for **3a** and **3b**, may lead to greater DNA affinity and enhanced potential for disrupting DNA functions, which is desirable for anti-cancer activity.

6. Conclusion

In summary, six new POCOP-Ni(II) complexes (**2**, **3a**, **3b**, **4**, **5**, and **6**) bearing morpholino-*s*-triazine moieties were synthesized and fully characterized. The structures of **2** and **3a** were determined by single-crystal X-ray diffraction (XRD) analysis, showing a distorted square-planar geometry of the metal centre. Supramolecular analysis of these structures was carried out through a Hirshfeld surface analysis and their related 2D fingerprint plots, revealing four main non-covalent interactions: C···H, O···H, N···H, and Cl···C. The intermolecular interaction appears as symmetrical 2D fingerprint plots.

Complexes **3a** and **3b** showed the highest antiproliferative activity, mainly against leukaemia (K562), with IC_{50} values of 0.55 μM for **3a** and 0.59 μM for **3b**. The higher activity could be associated with the morpholine fragment since the corres-

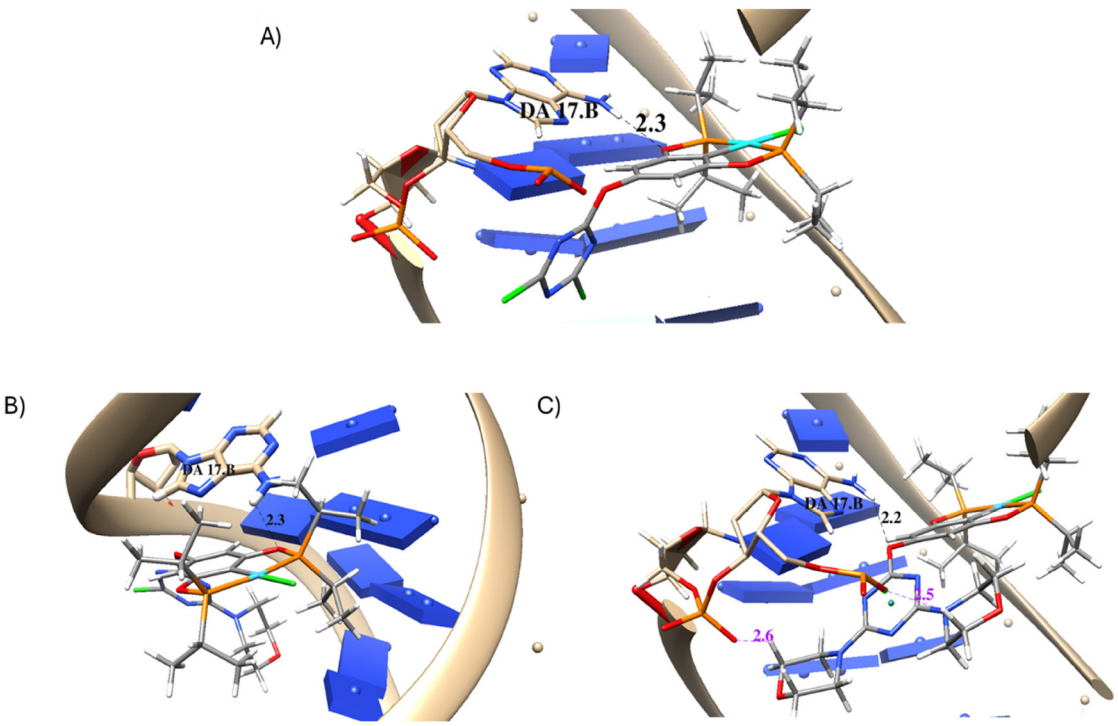

Fig. 7 Molecular interactions between DNA and (A) **2**, (B) **3a**, and (C) **3b** complexes. Color code: Ni (cyan), Cl (green), N (blue), C (gray), H (white), and O (red). Black dashed lines represent hydrogen bonds, and purple dashed lines indicate electrostatic interactions.

ponding analogue **2** without morpholine showed lower cytotoxic activity (4.96 μM). All three complexes could effectively displace EB from the DNA–EB adduct.

Molecular docking studies demonstrate that nickel complexes **3a** and **3b** exhibit strong potential as dual-target anticancer agents due to their high binding affinities for both DNA and phosphoinositide 3-kinase. The combination of hydrophobic and electrostatic interactions contributes significantly to their stability in the binding sites, particularly in DNA, where favorable electrostatic attractions with the phosphate backbone enhance complex stability. Unlike **2**, which experiences electrostatic repulsion with DNA, **3a** and **3b** achieve enhanced stability, suggesting their superior affinity and potential biological efficacy. These results highlight the promise of these nickel complexes as effective kinase and DNA-binding inhibitors, paving the way for further studies to optimize their therapeutic application in cancer treatment.

7. Experimental section

All chemical compounds were commercially obtained and used as received without further purification. The ^{1}H, $^{13}C\{^{1}H\}$, and $^{31}P\{^{1}H\}$ NMR spectra were obtained on a Bruker 500 Ascend spectrometer. Chemical shifts are reported in ppm downfield of TMS employing the residual signals in the solvent ($CDCl_3$) as the internal standard. ATR-IR measurements were performed on a FTIR NICOLET IS50, Thermo Fisher Scientific spectrometer. Elemental analyses were performed on a Thermo Scientific Flash 2000 elemental analyzer, using a Mettler Toledo XP6 Automated-S Microbalance and sulfanilamide as standard (Thermo Scientific BN 217826, attained values N = 16.40%, C = 41.91%, H = 4.65%, and S = 18.63%; certified values N = 16.26%, C = 41.81%, H = 4.71%, and S = 18.62%). DART-MS determinations were recorded using a JEOL AccuTOF JMS-T100LC mass spectrometer and MALDI-MS determinations were recorded using a Bruker Microflex TOF spectrometer with DHB 2/5 matrix. Complex **1** was synthesized according to the methodology previously designed by our investigation group, and was characterized by ^{1}H, ^{13}C, and ^{31}P NMR spectroscopy and elemental analysis, showing the expected results.[31] Stability studies were performed using a Shimadzu UV-2600 spectrophotometer (Shimadzu Corporation, Kyoto Japan) at 10 μM and 25 °C in a PBS solution (0.1% DMSO), following a reported methodology.[47]

7.1. Synthesis of compound 2

A round-bottomed flask was charged with 1.11 mmol of 2,4,6-trichloro-*s*-triazine (TCT), 0.56 mmol of diisopropylethylamine (DIPEA), and 40 mL of THF. Then, 20 mL of a solution of 0.22 mmol of **1** and 0.54 mmol of DIPEA were added dropwise at 0 °C. Afterwards, the reaction mixture was agitated for 5 h and allowed to reach room temperature. The crude product was purified on a chromatographic column using CH_2Cl_2 as the eluent. The compound was obtained as a yellow solid. Yield 89%. M.p. 201–204 °C. ^{1}H NMR (500 MHz, $CDCl_3$) δ 6.26 (s, 2H, C*H*Ar), 2.47–2.41 (m, 4H, C*H*$(CH_3)_2$), 1.47–1.34 (m, 24H, –CH(C*H*$_3)_2$). $^{13}C\{^{1}H\}$ NMR (125.7 MHz, $CDCl_3$) δ 173.2 (s, *C*–N), 171.0 (s, *C*–N), 168.5 (t, *C*–O, $^{2}J_{C-P}$ = 10.4 Hz), 151.6 (s, *C*–O), 123.6 (t, *C*–Ni, $^{2}J_{C-P}$ = 21.4 Hz), 98.8 (t, *C*–H, $^{3}J_{C-P}$ = 6.4 Hz), 28.0 (t, –*C*H$(CH_3)_2$, $^{1}J_{C-P}$ = 10.8 Hz), 17.6 (s, –*C*H$(CH_3)_2$), 16.9 (s, –*C*H$(CH_3)_2$). $^{31}P\{^{1}H\}$ NMR (202.4 MHz, $CDCl_3$): δ 188.41. MS (DART$^+$): *m*/*z* 600 $[M + H]^+$. IR (ATR, cm^{-1}): 1514 (s, C–N═C), 1114 (s, C–O–C). Elem. anal. calcd for $C_{21}H_{30}Cl_3N_3NiO_3P_2$: C, 42.07; H, 5.04; N, 7.01. Found: C, 42.64; H, 5.21; N, 7.17.

7.2. Synthesis of compound 3a

A round-bottomed flask was charged with 0.11 mmol of **2**, 0.22 mmol of DIPEA, 0.11 mmol of morpholine, and 25 mL of acetone. Then, the reaction mixture was allowed to react overnight at −5 °C. The crude product was purified on a chromatographic column using CH_2Cl_2 as the eluent. The compound was obtained as a yellow solid. Yield 74%. M.p. 212–215 °C. ^{1}H NMR (500 MHz, $CDCl_3$) δ 6.25 (s, 2H, C*H*Ar), 3.85 (m, 2H, CH_2), 3.71 (m, 2H, CH_2), 3.65 (m, 4H, CH_2), 2.44–2.41 (m, 4H, C*H*$(CH_3)_2$), 1.46–1.32 (m, 24H, –CH(C$H_3)_2$). $^{13}C\{^{1}H\}$ NMR (125.7 MHz, $CDCl_3$) δ 171.7 (s, *C*–N), 170.8 (s, *C*–N), 168.3 (t, *C*–O, $^{2}J_{C-P}$ = 10.3 Hz), 165.5 (s, *C*–N), 152.7 (s, *C*–O), 122.0 (t, *C*–Ni, $^{2}J_{C-P}$ = 21.9 Hz), 99.5 (t, *C*–H, $^{3}J_{C-P}$ = 6.3 Hz), 66.6 (s, –*C*H_2), 66.4 (s, –*C*H_2), 44.4 (s, –*C*H_2), 44.1 (s, –*C*H_2), 28.0 (t, –*C*H$(CH_3)_2$, $^{1}J_{C-P}$ = 10.8 Hz), 17.6 (s, –*C*H$(CH_3)_2$), 16.8 (s, –*C*H$(CH_3)_2$). $^{31}P\{^{1}H\}$ NMR (202.4 MHz, $CDCl_3$): δ 187.24. MS (DART$^+$): *m*/*z* 651 $[M + H]^+$. IR (ATR, cm^{-1}): 1569 (s, C–N), 1509 (s, C═N–C), 1113 (s, C–O–C). Elem. anal. calcd for $C_{25}H_{38}Cl_2N_4NiO_4P_2$: C, 46.19; H, 5.89; N, 8.62. Found: C, 45.88; H, 5.90; N, 8.21.

7.3. Synthesis of compound 3b

0.11 mmol **2**, 0.22 mmol of base DIPEA, and the corresponding amount of morpholine (0.22 mmol) were added to 30 mL of acetone in a round-bottomed flask. Then, the reaction mixture was refluxed overnight at 56 °C. The crude product was purified on a chromatographic column using CH_2Cl_2 as the eluent. The compound was obtained as a yellow solid. Yield 68%. M.p. 218–220 °C. ^{1}H NMR (500 MHz, $CDCl_3$) δ 6.25 (s, 2H, C*H*Ar), 3.85 (m, 2H, CH_2), 3.71 (m, 2H, CH_2), 3.65 (m, 4H, CH_2), 2.44–2.41 (m, 4H, C*H*$(CH_3)_2$), 1.46–1.32 (m, 24H, –CH(C$H_3)_2$). $^{13}C\{^{1}H\}$ NMR (125.7 MHz, $CDCl_3$) δ 171.7 (s, *C*–N), 170.8 (s, *C*–N), 168.3 (t, *C*–O, $^{2}J_{C-P}$ = 10.3 Hz), 165.5 (s, *C*–N), 152.7 (s, *C*–O), 122.0 (t, *C*–Ni, $^{2}J_{C-P}$ = 21.9 Hz), 99.5 (t, *C*–H, $^{3}J_{C-P}$ = 6.3 Hz), 66.6 (s, –*C*H_2), 66.4 (s, –*C*H_2), 44.4 (s, –*C*H_2), 44.1 (s, –*C*H_2), 28.0 (t, –*C*H$(CH_3)_2$, $^{1}J_{C-P}$ = 10.8 Hz), 17.6 (s, –*C*H$(CH_3)_2$), 16.8 (s, –*C*H$(CH_3)_2$). $^{31}P\{^{1}H\}$ NMR (202.4 MHz, $CDCl_3$): δ 187.24. MS (DART$^+$): 700 *m*/*z* $[M]^+$. IR (ATR, cm^{-1}): 1574 (s, C–N), 1497 (s, C═N–C), 1114 (s, C–O–C). Elem. anal. calcd for $C_{29}H_{46}ClN_5NiO_5P_2$: C, 49.70; H, 6.62; N, 9.99. Found: C, 49.87; H, 6.73; N, 9.65.

7.4. Synthesis of compound 4

A round-bottomed flask was charged with 0.11 mmol of **1**, 0.22 mmol of DIPEA, 0.06 mmol of 2,4,6-trichloro-*s*-triazine

(TCT), and 30 mL of CH_2Cl_2. Then, the reaction mixture was allowed to react overnight at room temperature. The crude product was purified on a chromatographic column using CH_2Cl_2 as the eluent. The compound was obtained as a yellow solid. Yield 78%. M.p. 279–282 °C. ^{1}H NMR (500 MHz, $CDCl_3$) δ 6.28 (s, 2H, C*H*Ar), 2.46–2.40 (m, 4H, C*H*$(CH_3)_2$), 1.47–1.33 (m, 24H, –CH(C*H*$_3)_2$). ^{13}C{^{1}H} NMR (125.7 MHz, $CDCl_3$) δ 173.7 (s, *C*–N), 172.3 (s, *C*–N), 168.5 (t, *C*–O, $^2J_{C-P}$ = 10.3 Hz), 152.0 (s, *C*–O), 123.0 (t, *C*–Ni, $^2J_{C-P}$ = 21.3 Hz), 99.1 (t, *C*–H, $^3J_{C-P}$ = 6.2 Hz), 28.0 (t, –*C*H$(CH_3)_2$, $^1J_{C-P}$ = 10.8 Hz), 17.6 (s, –*C*H$(CH_3)_2$), 16.9 (s, –*C*H$(CH_3)_2$). ^{31}P{^{1}H} NMR (202.4 MHz, $CDCl_3$): δ 187.91. MS (MALDI): *m*/*z* 1013 $[M]^+$, 978 $[M - Cl]^+$. IR (ATR, cm^{-1}): 1536 (s, C–N═C), 1115 (s, C–O–C). Elem. anal. calcd for $C_{39}H_{60}Cl_3N_3Ni_2O_6P_4$: C, 46.17; H, 5.96; N, 4.14. Found: C, 46.89; H, 6.17, N, 4.33.

7.5. Synthesis of compound 5

0.11 mmol **4**, 0.22 mmol of base DIPEA, and the corresponding amount of morpholine (0.11 mmol) were added to 30 mL of acetone in a round-bottomed flask. Then, the reaction mixture was refluxed overnight at 56 °C. The crude product was purified on a chromatographic column using CH_2Cl_2 as the eluent. The compound was obtained as a yellow solid. Yield 79%. M.p. 279–280 °C. ^{1}H NMR (500 MHz, $CDCl_3$) δ 6.28 (s, 2H, C*H*Ar), 3.63–3.60 (m, 4H, C*H*$_2$), 2.44–2.39 (m, 4H, C*H*$(CH_3)_2$), 1.45–1.31 (m, 24H, –CH(C*H*$_3)_2$). ^{13}C{^{1}H} NMR (125.7 MHz, $CDCl_3$) δ 172.5 (s, *C*–N), 168.3 (t, *C*–O, $^2J_{C-P}$ = 10.2 Hz), 166.7 (s, *C*–N), 153.1 (s, *C*–O), 121.5 (t, *C*–Ni, $^2J_{C-P}$ = 21.7 Hz), 99.7 (t, *C*–H, $^3J_{C-P}$ = 6.3 Hz), 66.5 (s, –*C*H$_2$), 44.0 (s, –*C*H$_2$), 28.0 (t, –*C*H$(CH_3)_2$, $^1J_{C-P}$ = 10.8 Hz), 17.6 (s, –*C*H$(CH_3)_2$), 16.8 (s, –*C*H$(CH_3)_2$). ^{31}P{^{1}H} NMR (202.4 MHz, $CDCl_3$): δ 186.82. MS (MALDI): *m*/*z* 1029 $[M - Cl]^+$. IR (ATR, cm^{-1}): 1852 (s, C–N), 1524 (s, C═N–C), 1127 (s, C–O–C). Elem. anal. calcd for $C_{43}H_{68}Cl_2N_4Ni2O_7P_4$: C, 48.49; H, 6.43; N, 5.26. Found: C, 48.66; H, 6.54; N, 5.25.

7.6. Synthesis of compound 6

0.11 mmol of **4**, 0.11 mmol of **1**, and 0.22 mmol of Na_2CO_3 were added to 30 mL of acetone in a round-bottomed flask. Then, the reaction mixture was refluxed overnight at 56 °C. The solvent was eliminated by vacuum evaporation. Afterwards, the product was purified by precipitation in hexane–ethyl acetate 2 : 1 and filtered. The solid was washed with 5 mL of water and 5 mL of acetone. The compound was obtained as a yellow solid. Yield 36%. M.p. > 300 °C. ^{1}H NMR (500 MHz, $CDCl_3$) δ 6.31 (s, 2H, C*H*Ar), 2.44–2.38 (m, 4H, C*H*$(CH_3)_2$), 1.46–1.32 (m, 24H, –CH(C*H*$_3)_2$). ^{13}C{^{1}H} NMR (125.7 MHz, $CDCl_3$) δ 173.6 (s, *C*–N), 168.4 (t, *C*–O), 152.3 (s, *C*–O), 122.5 (t, *C*–Ni), 99.3 (t, *C*–H, $^3J_{C-P}$ = 5.4 Hz), 28.0 (t, –*C*H$(CH_3)_2$, $^1J_{C-P}$ = 10.7 Hz), 17.6 (s, –*C*H$(CH_3)_2$), 16.9 (s, –*C*H$(CH_3)_2$). ^{31}P{^{1}H} NMR (202.4 MHz, $CDCl_3$): δ 187.91. MS (MALDI): *m*/*z* 1428 $[M]^+$, 1393 $[M - Cl]^+$. IR (ATR, cm^{-1}): 1557 (s, C═N–C), 1140 (s, C–O–C). Elem. anal. calcd for $C_{57}H_{90}Cl_3N_3Ni_3O_9P_6$: C, 47.89; H, 6.35; N, 2.94. Found: C, 48.32; H, 6.34, N, 3.30.

7.7. Cytotoxicity assay

The compounds were screened *in vitro* against human cancer cell lines: HCT-15 (human colorectal adenocarcinoma), MCF-7 (human mammary adenocarcinoma), K562 (human chronic myelogenous leukaemia), U251 (human glioblastoma), and PC-3 (human prostatic adenocarcinoma) cell lines supplied by the National Cancer Institute (USA); and SKLU-1 (human lung adenocarcinoma) and COS-7 (cell line from African green monkey kidney cells) cell lines donated by the Cancer Institute of Mexico. The cell lines were cultured in RPMI-1640 medium supplemented with 10% fetal bovine serum, 2 mM L-glutamine, 25 μg mL^{-1} amphotericin B (Gibco) and 1% non-essential amino acids (Gibco). They were maintained at 37 °C under a humidified atmosphere with 5% CO_2.

Cytotoxicity after treatment of the tumor cells and normal cells with the test compounds was determined using the protein-binding dye sulforhodamine B (SRB) in a microculture assay to measure cell growth.[48] The cells were exposed for 48 h to the compound at a concentration of 10 μM. DMSO was employed as a vehicle. After the incubation period, cells were fixed to the plastic substratum by the addition of 50 μL of cold 50% aqueous trichloroacetic acid. The plates were incubated at 4 °C for 1 h, washed with tap H_2O, and air-dried. The trichloroacetic-acid-fixed cells were stained by the addition of 0.4% SRB. Free SRB solution was removed by washing with 1% aqueous acetic acid. The plates were then air-dried, and the bound dye was solubilized by the addition of 10 mM unbuffered tris base (100 μL). The plates were placed on and shaken for 10 min, and the absorption was determined at 515 nm using an ELISA plate reader (Bio-Tex Instruments). The half-maximal inhibitory concentration (IC_{50}) values were calculated on extrapolated fit curves based on dose/response data analysed in triplicate for each compound through linear regression analysis.

7.8. Competitive displacement assay

Stock solutions of compounds **2**, **3a** and **3b** were dissolved in DMSO at concentrations of 0.01 M, 0.01 M and 0.005 M, respectively. The assay was performed in 3 mL of interaction buffer (5 mM Tris–HCl, 5 mM NaCl, pH 7.4, 2.5×10^{-5} ethidium bromide, and 1.25×10^{-4} M ss-DNA (SIGMA)).[49] Stock solutions were then titrated into the interaction buffer.[50] After incubation at 25 °C for 5 min, the fluorescence intensity of the samples was read (average of three readings) using an Agilent Cary Eclipse spectrofluorometer from 540 and 700 nm (λ_{ex} = 520 nm).

7.9. Computational details for compounds 2, 3a and 3b

The 3D structure of the **3b** complex was generated based on the crystal structure of the **3a** complex using Avogadro software.[51] To relax the crystal structure of complexes **2** and **3a**, we optimized them using the B3LYP DFT functional with the 6-31+G(d,p) basis set for all atoms. Solvent effects (water) were included using the SMD solvation model.[52] To verify that the

optimized geometry represents a true minimum on the potential energy surface. Finally, we calculated NBO charges at the same level of theory to obtain atomic charges for the Ni atom,[53] which were used to parameterize it for subsequent molecular docking studies. All electronic calculations were conducted using Gaussian 16.[54]

To study the anti-cancer activity of the Ni complex, we selected two targets. The first target was DNA (PDB code 1AIO),[55] aimed at activating the DNA repair pathway, using cisplatin as a reference. The second target was phosphoinositide 3-kinases (PI3Ks) (PDB code 5JHB),[46] also known as phosphatidylinositol 3-kinases, which are involved in cellular functions such as cell growth and proliferation, with inhibitor 6K5 as a reference. For both targets, Gasteiger charges[56] were added using AutoDockTools 4.[57] NBO charges were added to the Ni complex PDBQT files to ensure accurate charge representation. To validate docking accuracy, we performed redocking using AutoDock 4,[57] employing a ligand from each target's crystal structure. Finally, the results were analyzed using Chimera[58] and Maestro software.[59]

7.10. Crystal structure determination for compounds 2 and 3a

Crystals of complex **2** were grown by slow evaporation from a 1 : 1 CH_2Cl_2/hexane solution, and crystals of complex **3a** were grown from a 2 : 1 hexane/acetyl acetate solution. Complex **2** was characterized on a Bruker D8 Venture diffractometer equipped with a Mo-Kα X-ray source (λ = 0.71073 Å). Cell parameters were determined using the Bruker SAINT. Hydrogen atoms were input at calculated positions and allowed to ride on the atoms to which they were attached. Thermal parameters were refined for hydrogen atoms on the phenyl groups using a U_{eq} = 1.2 Å to the precedent atom. Absorption corrections were applied using the SADABS program.[60] Complex **3a** was characterized on an Oxford Diffraction Gemini diffractometer equipped with a Mo-Kα X-ray source (λ = 0.71073 Å). CrysAlisPro and CrysAlis RED software packages were used for data collection and integration.[61] Structure solutions and refinements were carried out with the SHELXS-2018 and SHELXL-2019 packages.[62,63]

Conflicts of interest

The authors declare no conflicts of interest.

Data availability

The data supporting this article have been included as part of the supplementary information (SI). Supplementary information is available. See DOI: https://doi.org/10.1039/d5dt01322d.

CCDC 2456663 (**2**) and 2456176 (**3a**) contain the supplementary crystallographic data for this paper.[64a,b]

Acknowledgements

A. A.-C expresses gratitude to CONAHCyT for the postdoctoral fellowships awarded under the "Estancias Posdoctorales por México 2021(1)" program. J. S. S.-G., and A. A.-F are grateful for the doctoral fellowships with CVU 997800 and 1032866, respectively. D. M. M. acknowledges the financial support for this research provided by PAPIIT-DGAPA-UNAM (PAPIIT IN223323) and CONAHCyT (A1-S-033933). Special thanks are extended to Jordi Ruiz-Galindo and Adrián Ruíz-Martínez for their important contribution for reviewing the manuscript, Elkin Sanchez-Yocue for his invaluable help to perform the stability studies, and María de La Paz Orta Pérez for running the elemental analyses.

References

1 H.-H. Han, H.-M. Wang, P. Jangili, M. Li, L. Wu, Y. Zang, A. C. Sedgwick, J. Li, X.-P. He, T. D. James and J. S. Kim, *Chem. Soc. Rev.*, 2023, **52**, 879–920.
2 F. Bray, M. Laversanne, H. Sung, J. Ferlay, R. L. Siegel, I. Soerjomataram and A. Jemal, *CA Cancer J. Clin.*, 2024, **74**, 229–263.
3 M. Shanmugam, K. Narayanan, K. H. Prasad, D. Karthikeyan, L. Chandrasekaran, R. Atchudan and V. Chidambaranathan, *New J. Chem.*, 2018, **42**, 1698–1714.
4 S. Ghosh, *Bioorg. Chem.*, 2019, **88**, 102925.
5 R. López-Sánchez, J. R. Pioquinto-Mendoza, L. González-Sebastián, R. A. Toscano, M. Flores-Alamo, M. Teresa Ramírez-Apan, A. L. Orjuela, J. Alí-Torres and D. Morales-Morales, *Inorg. Chim. Acta*, 2023, **550**, 121450.
6 A. Aragón-Muriel, B. A. Aguilar-Castillo, E. Rufino-Felipe, H. Valdés, L. González-Sebastián, R. N. Osorio-Yáñez, Y. Liscano, V. Gómez-Benítez, D. Polo-Cerón and D. Morales-Morales, *Polyhedron*, 2022, **227**, 116115.
7 A. A. Castillo-García, L. González-Sebastián, L. Lomas-Romero, S. Hernandez-Ortega, R. A. Toscano and D. Morales-Morales, *New J. Chem.*, 2021, **45**, 10204–10216.
8 J. S. Serrano-García, A. Amaya-Flórez, J. R. Galindo, L. González-Sebastián, L. H. Delgado-Rangel and D. Morales-Morales, *Inorganics*, 2024, **12**, 221.
9 K. J. Szabó and O. F. Wendt, *Pincer and pincer-type complexes: Applications in organic synthesis and catalysis*, John Wiley & Sons, Weinheim, 2014.
10 R. P. Hausinger, B. Desguin, M. Fellner, J. A. Rankin and J. Hu, *Curr. Opin. Chem. Biol.*, 2018, **47**, 18–23.
11 J. A. Rankin, R. C. Mauban, M. Fellner, B. Desguin, J. McCracken, J. Hu, S. A. Varganov and R. P. Hausinger, *Biochemistry*, 2018, **57**, 3244–3251.
12 A. Sánchez-Mora, E. Briñez, A. Pico, L. González-Sebastián, J. Antonio Cruz-Navarrro, A. Arenaza-Corona, N. Puentes-Díaz, J. Alí-Torres, V. Reyes-Márquez and D. Morales-Morales, *Chem. Biodiversity*, 2024, **21**, e202400995.
13 A. Amaya-Flórez, J. S. Serrano-García, J. Ruiz-Galindo, A. Arenaza-Corona, J. A. Cruz-Navarro, A. L. Orjuela, J. Alí-

Torres, M. Flores-Alamo, P. Cano-Sanchez, V. Reyes-Márquez and D. Morales-Morales, *Front. Chem.*, 2014, **12**, DOI: 10.3389/fchem.2024.1483999.
14 S. Abdolmaleki, S. Khaksar, A. Aliabadi, A. Panjehpour, E. Motieiyan, D. Marabello, M. H. Faraji and M. Beihaghi, *Toxicology*, 2023, **492**, 153516.
15 H. Y. Lim and A. V. Dolzhenko, *Eur. J. Med. Chem.*, 2024, **276**, 116680.
16 S. Cascioferro, B. Parrino, V. Spanò, A. Carbone, A. Montalbano, P. Barraja, P. Diana and G. Cirrincione, *Eur. J. Med. Chem.*, 2017, **142**, 523–549.
17 S. Jain, P. K. Jain, S. Sain, D. Kishore and J. Dwivedi, *Mini-Rev. Org. Chem.*, 2020, **17**, 904–921.
18 R. Fiorot, R. Westphal, B. Lemos, R. Romagna, P. Gonçalves, M. Fernandes, C. Ferreira, A. Taranto and S. Greco, *J. Braz. Chem. Soc.*, 2019, **30**, 1860–1873.
19 S. Singh, M. K. Mandal, A. Masih, A. Saha, S. K. Ghosh, H. R. Bhat and U. P. Singh, *Arch. Pharm.*, 2021, **354**, e2000363.
20 M. Balaha, M. El-Hamamsy, N. El-Din and N. A. El-Mahdy, *J. Appl. Pharm. Sci.*, 2016, **6**, 028–045.
21 P. Prasher, M. Sharma, A. A. A. Aljabali, G. Gupta, P. Negi, D. N. Kapoor, I. Singh, F. C. Zacconi, T. de Jesus Andreoli Pinto, M. W. da Silva, H. A. Bakshi, D. K. Chellappan, M. M. Tambuwala and K. Dua, *Drug Dev. Res.*, 2020, **81**, 837–858.
22 P. Kumari, S. Kaur, J. Kaur, R. Bhatti and P. Singh, *Bioorg. Med. Chem.*, 2020, **28**, 115246.
23 S. Yaguchi, Y. Fukui, I. Koshimizu, H. Yoshimi, T. Matsuno, H. Gouda, S. Hirono, K. Yamazaki and T. Yamori, *J. Natl. Cancer Inst.*, 2006, **98**, 545–556.
24 M. S. Miller, J.-A. Pinson, Z. Zheng, I. G. Jennings and P. E. Thompson, *Bioorg. Med. Chem. Lett.*, 2013, **23**, 802–805.
25 S. Toyama, N. Tamura, K. Haruta, T. Karakida, S. Mori, T. Watanabe, T. Yamori and Y. Takasaki, *Arthritis Res. Ther.*, 2010, **12**, R92.
26 F. Beaufils, N. Cmiljanovic, V. Cmiljanovic, T. Bohnacker, A. Melone, R. Marone, E. Jackson, X. Zhang, A. Sele, C. Borsari, J. Mestan, P. Hebeisen, P. Hillmann, B. Giese, M. Zvelebil, D. Fabbro, R. L. Williams, D. Rageot and M. P. Wymann, *J. Med. Chem.*, 2017, **60**, 7524–7538.
27 M. A. Sk, K. Hemalatha, G. S. P. Matada, R. Pal, B. V. Manjushree, S. Mounika, E. Haripiya, M. P. Viji and D. Anjan, *Bioorg. Chem.*, 2025, **154**, 108011.
28 A. P. Kourounakis, D. Xanthopoulos and A. Tzara, *Med. Res. Rev.*, 2020, **40**, 709–752.
29 A. Kumari and R. K. Singh, *Bioorg. Chem.*, 2020, **96**, 103578.
30 B. Saroha, G. Kumar, P. Arya, N. Raghav and S. Kumar, *Bioorg. Chem.*, 2023, **140**, 106805.
31 M. A. García-Eleno, E. Padilla-Mata, F. Estudiante-Negrete, F. Pichal-Cerda, S. Hernández-Ortega, R. A. Toscano and D. Morales-Morales, *New J. Chem.*, 2015, **39**, 3361–3365.
32 J. S. Serrano-García, M. A. García-Eleno, A. Arenaza-Corona, E. Rufino-Felipe, H. Valdes, S. Hernandez-Ortega and D. Morales-Morales, *Dalton Trans.*, 2025, **54**, 694–699.
33 O. V. Dolomanov, L. J. Bourhis, R. J. Gildea, J. A. K. Howard and H. Puschmann, *J. Appl. Crystallogr.*, 2009, **42**, 339–341.
34 C. F. Macrae, I. Sovago, S. J. Cottrell, P. T. A. Galek, P. McCabe, E. Pidcock, M. Platings, G. P. Shields, J. S. Stevens, M. Towler and P. A. Wood, *J. Appl. Crystallogr.*, 2020, **53**, 226–235.
35 J. Bernstein, R. E. Davis, L. Shimoni and N. Chang, *Angew. Chem., Int. Ed. Engl.*, 1995, **34**, 1555–1573.
36 J. J. McKinnon, D. Jayatilaka and M. A. Spackman, *Chem. Commun.*, 2007, 3814–3816.
37 P. R. Spackman, M. J. Turner, J. J. McKinnon, S. K. Wolff, D. J. Grimwood, D. Jayatilaka and M. A. Spackman, *J. Appl. Crystallogr.*, 2021, **54**, 1006–1011.
38 M. A. Spackman and J. J. McKinnon, *CrystEngComm*, 2002, **4**, 378–392.
39 S. Suda, A. Tateno, D. Nakane and T. Akitsu, *Int. J. Org. Chem.*, 2023, **13**, 57–85.
40 M. Małecka and E. Budzisz, *CrystEngComm*, 2014, **16**, 6654–6663.
41 M. Małecka, J. Kusz, L. Eriksson, A. Adamus-Grabicka and E. Budzisz, *Acta Crystallogr., Sect. C:Struct. Chem.*, 2020, **76**, 723–733.
42 B. Kupcewicz, M. Małecka, M. Zapadka, U. Krajewska, M. Rozalski and E. Budzisz, *Bioorg. Med. Chem. Lett.*, 2016, **26**, 3336–3341.
43 O. De Henau, M. Rausch, D. Winkler, L. F. Campesato, C. Liu, D. Hirschhorn-Cymerman, S. Budhu, A. Ghosh, M. Pink, J. Tchaicha, M. Douglas, T. Tibbitts, S. Sharma, J. Proctor, N. Kosmider, K. White, H. Stern, J. Soglia, J. Adams, V. J. Palombella, K. McGovern, J. L. Kutok, J. D. Wolchok and T. Merghoub, *Nature*, 2016, **539**, 443–447.
44 M. M. Kaneda, P. Cappello, A. V. Nguyen, N. Ralainirina, C. R. Hardamon, P. Foubert, M. C. Schmid, P. Sun, E. Mose, M. Bouvet, A. M. Lowy, M. A. Valasek, R. Sasik, F. Novelli, E. Hirsch and J. A. Varner, *Cancer Discovery*, 2016, **6**, 870–885.
45 M. K. Rathinaswamy, U. Dalwadi, K. D. Fleming, C. Adams, J. T. B. Stariha, E. Pardon, M. Baek, O. Vadas, F. DiMaio, J. Steyaert, S. D. Hansen, C. K. Yip and J. E. Burke, *Sci. Adv.*, 2021, **7**, eabj4282.
46 T. Bohnacker, A. E. Prota, F. Beaufils, J. E. Burke, A. Melone, A. J. Inglis, D. Rageot, A. M. Sele, V. Cmiljanovic, N. Cmiljanovic, K. Bargsten, A. Aher, A. Akhmanova, J. F. Díaz, D. Fabbro, M. Zvelebil, R. L. Williams, M. O. Steinmetz and M. P. Wymann, *Nat. Commun.*, 2017, **8**, 14683.
47 M. I. Murillo, C. F. Mejia, A. Restrepo-Acevedo, B. Barraud, A. L. Orjuela, M. Flores-Alamo, R. A. Toscano, J. Alí-Torres, A. D. Ryabov and R. Le Lagadec, *Inorganics*, 2025, **13**, 198.
48 V. Vichai and K. Kirtikara, *Nat. Protoc.*, 2006, **1**, 1112–1116.
49 G. Backman-Blanco, H. Valdés, M. T. Ramírez-Apan, P. Cano-Sanchez, S. Hernandez-Ortega, A. L. Orjuela, J. Alí-Torres, A. Flores-Gaspar, R. Reyes-Martínez and D. Morales-Morales, *J. Inorg. Biochem.*, 2020, **211**, 111206.

50 A. Banerjee, J. Singh and D. Dasgupta, *J. Fluoresc.*, 2013, **23**, 745–752.
51 M. D. Hanwell, D. E. Curtis, D. C. Lonie, T. Vandermeerschd, E. Zurek and G. R. Hutchison, *J. Cheminf.*, 2012, **4**, 1–17.
52 A. V. Marenich, C. J. Cramer and D. G. Truhlar, *J. Phys. Chem. B*, 2009, **113**, 6378–6396.
53 E. D. Glendening, C. R. Landis and F. Weinhold, *J. Comput. Chem.*, 2013, **34**, 1429–1437.
54 M. J. Frisch, G. W. Trucks, H. B. Schlegel, G. E. Scuseria, M. A. Robb, J. R. Cheeseman, G. Scalmani, V. Barone, G. A. Petersson, H. Nakatsuji, X. Li, M. Caricato, A. V. Marenich, J. Bloino, B. G. Janesko, R. Gomperts, B. Mennucci, H. P. Hratchian, J. V. Ortiz, A. F. Izmaylov, J. L. Sonnenberg, D. Williams-Young, F. Ding, F. Lipparini, F. Egidi, J. Goings, B. Peng, A. Petrone, T. Henderson, D. Ranasinghe, V. G. Zakrzewski, J. Gao, N. Rega, G. Zheng, W. Liang, M. Hada, M. Ehara, K. Toyota, R. Fukuda, J. Hasegawa, M. Ishida, T. Nakajima, Y. Honda, O. Kitao, H. Nakai, T. Vreven, K. Throssell, J. A. Montgomery Jr., J. E. Peralta, F. Ogliaro, M. J. Bearpark, J. J. Heyd, E. N. Brothers, K. N. Kudin, V. N. Staroverov, T. A. Keith, R. Kobayashi, J. Normand, K. Raghavachari, A. P. Rendell, J. C. Burant, S. S. Iyengar, J. Tomasi, M. Cossi, J. M. Millam, M. Klene, C. Adamo, R. Cammi, J. W. Ochterski, R. L. Martin, K. Morokuma, O. Farkas, J. B. Foresman and D. J. Fox, *Gaussian 16, Revision D.01*, 2016.
55 P. M. Takahara, A. C. Rosenzweig, C. A. Frederick and S. J. Lippard, *Nature*, 1995, **377**, 649–652.
56 J. Gasteiger and M. Marsili, *Tetrahedron*, 1980, **36**, 3219–3288.
57 G. Morris and R. Huey, *J. Comput. Chem.*, 2009, **30**, 2785–2791.
58 E. F. Pettersen, T. D. Goddard, C. C. Huang, G. S. Couch, D. M. Greenblatt, E. C. Meng and T. E. Ferrin, *J. Comput. Chem.*, 2004, **25**, 1605–1612.
59 *Schrödinger Release 2023-2, Maestro*, LLC, New York, 2023.
60 L. Krause, R. Herbst-Irmer, G. M. Sheldrick and D. Stalke, *J. Appl. Crystallogr.*, 2015, **48**, 3–10.
61 Oxford Diffraction, Xcalibur CCD System, *CrysAlis CCD and CrysAlis RED, Versions 1.171.36.32*, Oxford Diffraction Ltd, Abingdon, UK, 2013.
62 Bruker AXS Inc, 2018.
63 G. M. Sheldrick, *Acta Crystallogr., Sect. C:Struct. Chem.*, 2015, **71**, 3–8.
64 (*a*) CCDC 2456663: Experimental Crystal Structure Determination, 2025, DOI: 10.5517/ccdc.csd.cc2ngc6q; (*b*) CCDC 2456176: Experimental Crystal Structure Determination, 2025, DOI: 10.5517/ccdc.csd.cc2nfvhg.